Electronic Delocalization in Discotic Liquid Crystals: A Joint Experimental and Theoretical Study

ARTICLE *in* JOURNAL OF THE AMERICAN CHEMICAL SOCIETY · SEPTEMBER 2004

Impact Factor: 12.11 · DOI: 10.1021/ja048669j · Source: PubMed

J|A|C|S
ARTICLES
Published on Web 09/04/2004

Electronic Delocalization in Discotic Liquid Crystals: A Joint Experimental and Theoretical Study

Xavier Crispin,*[,†,||] Jérôme Cornil,[‡,§] Rainer Friedlein,[†] Koji Kamiya Okudaira,[▽] Vincent Lemaur,[‡] Annica Crispin,[†] Gaël Kestemont,[⊥] Matthias Lehmann,[⊥] Mats Fahlman,[||] Roberto Lazzaroni,[‡,§] Yves Geerts,[⊥] Göran Wendin,[#] Nobuo Ueno,[▽] Jean-Luc Brédas,[‡,§] and William R. Salaneck[†]

Contribution from the Department of Physics and Measurement Technology, IFM, Linköping University, S-58183 Linköping, Sweden, Service de Chimie des Matériaux Nouveaux, Centre de Recherche en Electronique et Photonique Moléculaires, Université de Mons-Hainaut, Place du Parc 20, B-7000 Mons, Belgium, School of Chemistry and Biochemistry, Georgia Institute of Technology, Atlanta, Georgia 30332-0400, Laboratoire de Chimie des Polymères, CP 206/1, Université Libre de Bruxelles, Boulevard du Triomphe, B-1050 Bruxelles, Belgium, Department of Science and Technology, Campus Norrköping, Linköping University, S-60174 Norrköping, Sweden, Department of Microtechnology and Nanoscience, MC2, Chalmers University of Technology, S-412 96 Göteborg, Sweden, and Department of Materials Science, Faculty of Engineering, Chiba University, Yayoi-cho, Inage-ku, Chiba 263-8522, Japan

Received March 8, 2004; E-mail: xavcr@itn.liu.se

Abstract: Discotic liquid crystals emerge as very attractive materials for organic-based (opto)electronics as they allow efficient charge and energy transport along self-organized molecular columns. Here, angle-resolved photoelectron spectroscopy (ARUPS) is used to investigate the electronic structure and supramolecular organization of the discotic molecule, hexakis(hexylthio)diquinoxalino[2,3-*a*:2′,3′-*c*]phenazine, deposited on graphite. The ARUPS data reveal significant changes in the electronic properties when going from disordered to columnar phases, the main feature being a decrease in ionization potential by 1.8 eV following the appearance of new electronic states at low binding energy. This evolution is rationalized by quantum-chemical calculations performed on model stacks containing from two to six molecules, which illustrate the formation of a quasi-band structure with Bloch-like orbitals delocalized over several molecules in the column. The ARUPS data also point to an energy dispersion of the upper π-bands in the columns by some 1.1 eV, therefore highlighting the strongly delocalized nature of the π-electrons along the discotic stacks.

1. Introduction

Discotic liquid crystals are currently widely considered for applications in organic-based (opto)electronic devices, such as light-emitting devices,[1−3] field-effect transistors,[4] solar cells,[5,6] and sensors.[7] This originates from their unique combination of properties: (i) the molecules, typically made of a central conjugated core substituted by saturated chains, are highly soluble and easily processed into organic thin films by spin-coating or ink-jet printing;[8] (ii) structural defects can be repaired by the self-healing properties of liquid crystal phases; (iii) the materials can be highly purified to eliminate impurities and/or chemical defects that are detrimental for charge transport; (iv) a high (supra)molecular order can be spontaneously achieved in films,[4,9] leading to charge mobilities in the discotic phase comparable to those in amorphous silicon (around 0.1 $cm^2/V \cdot s$),[10,11] i.e., up to 3 orders of magnitude larger than typical values in conjugated polymers; and (v) the exciton diffusion length, a highly relevant parameter for sensors and photovoltaic applications, is 1 order of magnitude larger than in conjugated polymers.[12,13]

[†] Department of Physics and Measurement Technology, Linköping University.
[‡] Université de Mons-Hainaut.
[§] Georgia Institute of Technology.
[⊥] Université Libre de Bruxelles.
[||] Department of Science and Technology, Linköping University.
[#] Chalmers University of Technology.
[▽] Chiba University.

(1) Lüssem, G.; Wendorff, J. H. *Polym. Adv. Technol.* **1998**, *9*, 443−460.
(2) Seguy, I.; Destruel, P.; Boch, H. *Synth. Met.* **2000**, *111*−*112*, 15−18.
(3) Seguy, I.; Jolinat, P.; Destruel, P.; Farenc, J.; Mamy, R.; Bock, H.; Ip, J.; Nguyen, T. P. *J. Appl. Phys.* **2001**, *89*, 5442−5448.
(4) Stutzmann, N.; Friend, R. H.; Sirringhaus, H. *Science* **2003**, *299*, 1881−1884.
(5) Schmidt-Mende, L.; Fechtenkötter, A.; Müllen, K.; Moons, E.; Friend, R. H.; MacKenzie, J. D. *Science* **2001**, *293*, 1119−1122.
(6) Schmidt-Mende, L.; Fechtenkotter, A.; Mullen, K.; Friend, R. H.; MacKenzie, J. D. *Physica E* **2002**, *14*, 263−267.
(7) Boden, N.; Bushby, R. J.; Clements, J.; Movaghar, B. *J. Mater. Chem.* **1999**, *9*, 2081−2086.
(8) Simpson, C. D.; Wu, J.; Watson, M. D.; Müllen, K. *J. Mater. Chem.* **2004**, *14*, 494−504.
(9) Zimmermann, S.; Wendorff, J. H.; Weder, C. *Chem. Mater.* **2002**, *14*, 2218−2223.
(10) Craats, A. M. v. d.; Warman, J. M.; Fechtenkötter, A.; Brand, J. D.; Harbison, M. A.; Müllen, K. *Adv. Mater.* **1999**, *11*, 1469−1472.
(11) Craats, A. M. v. d.; Warman, J. M. *Adv. Mater.* **2001**, *13*, 130−133.
(12) Markovitsi, D.; Marguet, S.; Gallos, L. K.; Sigal, H.; Millié, P.; Argyrakis, P.; Ringsdorf, H.; Kumar, S. *Chem. Phys. Lett.* **1999**, *306*, 163−167.

Discotic molecules are known to pack into one-dimensional columns in both the crystalline and liquid crystalline phases. The molecular organization in thin films is influenced by the substrate[14,15] and can therefore be different than in the bulk. The formation of such columns is governed by the strong intermolecular interactions among the cores and among lateral chains of adjacent units and induces an efficient one-dimensional charge transport along the stacks. Recent theoretical studies have pointed out the main parameters controlling the charge mobility in organic semiconductors at the molecular scale[16] and, in particular, in π-conjugated discotic liquid crystals.[17−20] Due to the large degree of geometric fluctuations within the columns, leading to modulations in the inter-disk distance and/or rotations of the disks around the stacking axis,[21] charge transport in discotic liquid crystals is usually expected to correspond to a phonon-assisted hopping regime, as is the case in amorphous organic thin films[22] or molecular crystals at high temperature.[23] In such a regime, the charges are localized over a single molecule and jump from site to site to yield a current. A major parameter governing the charge mobility, be it in a (localized) hopping or (delocalized) band regime, is the transfer integral t. The transfer integral describes the strength of the interactions between adjacent molecules and can be estimated to a very good approximation for hole [electron] transport as half the splitting of the highest occupied molecular orbital, HOMO [lowest unoccupied molecular orbital, LUMO], level in a dimer made of two neutral molecules.[16,24−26] In the context of a tight-binding model, the widths of the valence and conduction bands of a neutral infinite stack equal 4 times the corresponding transfer integrals.[16,25,27] The width of the valence band can be probed by ultraviolet photoelectron spectroscopy (UPS). Similar considerations apply to the conduction band; however, the latter is less accessible at the experimental level.

Here, we study by means of angle-resolved ultraviolet photoelectron spectroscopy (ARUPS) the electronic structure of hexakis(hexylthio)diquinoxalino[2,3-*a*:2′,3′-*c*]phenazine (HATNA-SC_6) molecules and its evolution when the molecules order into columns upon heating in ultrahigh vacuum. The choice of HATNA derivatives is motivated by their very good transport properties; the sum of the hole and electron mobilities varies from 0.01 to 0.6 cm^2/Vs at room temperature, depending on the alkyl chain length.[28] This discotic molecule is larger than the well-known triphenylene molecule and incorporates six nitrogen atoms within the conjugated core (Figure 1a). Note that UPS allows us to probe the electronic structure of the columns in the geometric structure characteristic of the neutral state, since the photoemission process is much faster ($\sim 10^{-16}$ s) than the nuclear geometry relaxation induced by the creation of the photohole ($\sim 10^{-14}-10^{-13}$ s). The spectroscopic data are interpreted with the help of the independent atomic center approximation[29] in order to shed light onto the preferential molecular orientation in the films, and with quantum-chemical calculations performed on the isolated molecule and model stacks containing from two to six molecules in order to characterize the π-electron delocalization.

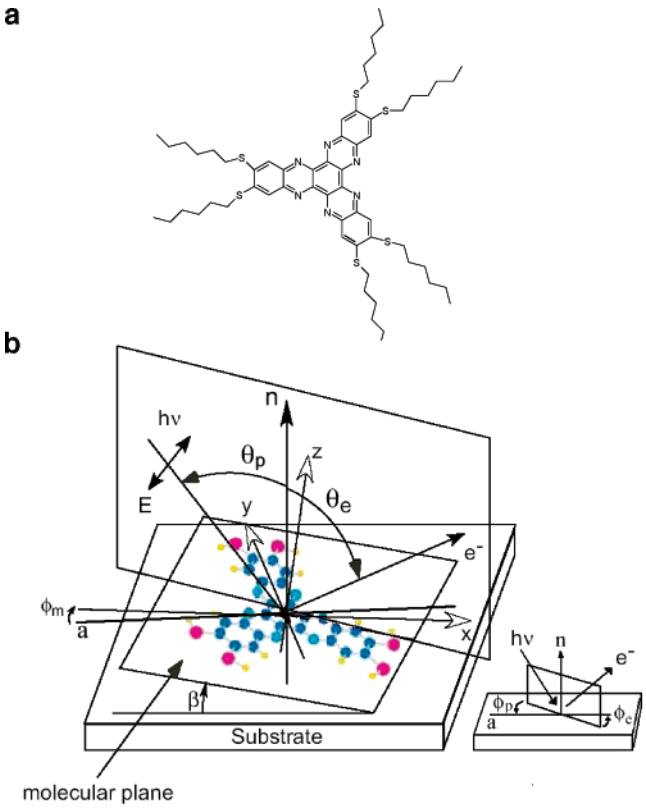

Figure 1. (a) Chemical structure of the HATNA-SC_6 molecule. (b) Geometry of the ARUPS experiments. ϕ_e and ϕ_p are the azimuthal angles for electrons and photons, respectively. θ_e and θ_p are the polar angles for electrons and photons, respectively, defined with respect to the surface normal. The position of the molecule is defined by two angles: the molecular tilt angle β with respect to the surface and the molecular azimuthal angle ϕ_m.

2. Experimental Section

The synthesis of the HATNA-SC_6 molecules has been reported earlier.[30] Six alkyl side chains, composed of six carbon atoms each, are attached via a sulfur atom to the HATNA conjugated core. The purity of the material used in this work is better than 99%. The impurities observed by nuclear magnetic resonance (^{1}H NMR) are nonconjugated solvent residues remaining from the purification by

(13) Markovitsi, D.; Gallos, L. K.; Lemaistre, J. P.; Argyrakis, P. *Chem. Phys.* **2001**, *269*, 147−158.
(14) Ruffieux, P.; Gröning, O.; Bielmann, M.; Simpson, C.; Müllen, K.; Schlapbach, L.; Gröning, P. *Phys. Rev. B* **2002**, *66*, 0734091−0734094.
(15) Friedlein, R.; Crispin, X.; Simpson, C.; Jäckel, F.; Osikowicz, W.; Marciniak, S.; Jong, M. P. d.; Jönsson, S. K. M.; Samori, P.; Fahlman, M.; Watson, M.; Müllen, K.; Rabe, J. P.; Salaneck, W. R. *Phys. Rev. B* **2003**, *68*, 195414−195417.
(16) Brédas, J. L.; Calbert, J. P.; Filho, D. A. d. S.; Cornil, J. *Proc. Natl. Acad. Sci., U.S.A.* **2002**, *99*, 5804−5809.
(17) Cornil, J.; Lemaur, V.; Calbert, J. P.; Brédas, J. L. *Adv. Mater.* **2002**, *14*, 726−729.
(18) Lemaur, V.; Filho, D. A. d. S.; Coropceanu, V.; Lehmann, M.; Geerts, Y.; Piris, J.; Debije, M. G.; Craats, A. M. v. d.; Senthilkumar, K.; Siebbeles, L. D. A.; Warman, J. M.; Brédas, J.-L.; Cornil, J. *J. Am. Chem. Soc.* **2004**, *126*, 3271−3279.
(19) Senthilkumar, K.; Grozema, F. C.; Bickelhaup, F. M.; Siebbeles, L. D. A. *J. Chem. Phys.* **2003**, *119*, 9809−9817.
(20) Palenberg, M. A.; Silbey, R. J.; Malagoli, M.; Brédas, J. L. *J. Chem. Phys.* **2000**, *112*, 1541−1546.
(21) Fischbach, I.; Pakula, T.; Minkin, P.; Fechtenkötter, A.; Müllen, K.; Spiess, H. W.; Saalwächter, K. *J. Phys. Chem. B* **2002**, *106*, 6408−6418.
(22) Bässler, H. *Phys. Stat. Solidi B* **1993**, *175*, 15−18.
(23) Duke, C.; Schein, L. *Phys. Today* **1980**, *33*, 42−48.
(24) Li, X. Y.; Tang, X. S.; He, F. C. *Chem. Phys.* **1999**, *248*, 137−146.
(25) Cornil, J.; Beljonne, D.; Calbert, J. P.; Brédas, J. L. *Adv. Mater.* **2001**, *13*, 1053−1067.
(26) Cornil, J.; Calbert, J. P.; Beljonne, D.; Silbey, R.; Brédas, J. L. *Synth. Met.* **2001**, *119*, 1−6.
(27) Salem, L. *The molecular theory of conjugated systems*; W. A. Benjamin, Inc.: New York, 1966.
(28) Warman, J.; Piris, J.; Debije, M., personal communication.
(29) Grobman, W. D. *Phys. Rev. B* **1978**, *17*, 4573−4585.
(30) Kestemont, G.; Halleux, V. d.; Lehmann, M.; Ivanov, D. A.; Watson, M.; Geerts, Y. H. *Chem. Commun.* **2001**, 2074−2075.

column chromatography. No large aromatic side products are detected by thin-layer chromatography. The films are formed by evaporating, at room temperature, a drop of a HATNA-SC_6/$CHCl_3$ (0.1 mg/mL) solution deposited onto a freshly cleaved highly oriented pyrolytic graphite (0001) surface (ZYB Bquality) or on a naturally oxidized silicon (100) surface (previously cleaned in an ultrasonic bath of acetone and 2-propanol). The thickness of the thin films is estimated from the suppression of the substrate core-level line by additional X-ray photoelectron spectroscopy measurements and is typically around 100−200 Å.

The angle-integrated UPS measurements have been carried out in Linköping with a spectrometer of our own design and construction, with a base pressure less than 1×10^{-9} mbar. The UPS spectra are recorded using monochromatized He I (21.2 eV) and He II (40.8 eV) radiations from a helium discharge lamp. The energy resolution is estimated to ±0.1 eV, as determined by the width of the gold Fermi edge. The work function is determined by the position of the secondary electron cutoff.

The angle-resolved photoelectron spectra have been recorded at beamline 41 of MAX-I at the MAX-Laboratory for Synchrotron Radiation Research in Lund, Sweden. The overall energy resolution is about 100 meV for an angular resolution of about 2°. The geometry of the ARUPS experiment is sketched in Figure 1b. The electric field vector of the incident photon beam, the surface normal, and the sample−detector axis are kept in the same plane. In other words, the azimuthal angles for ejected electrons, ϕ_e, and incident photons, ϕ_p, relative to a reference axis *a* on the surface are the same and kept constant. In all of the measurements, the photon beam hits the surface at grazing incidence with a polar angle $\theta_p = 80°$, while the photoelectrons are collected at a chosen polar angle θ_e. The binding energies refer to the vacuum level, as obtained by adding the work function of the samples to the energy scale of the UPS spectra initially measured with respect to the Fermi level.

3. Theoretical Approach

The model molecule HATNA-SH chosen for the electronic structure calculations has the same conjugated core as the actual HATNA-SC_6 discotic liquid crystal molecules. The geometric structure of the HATNA-SH molecule has been optimized at the density functional theory (DFT) level using the B3LYP functionals and a 6-31g(d,p) basis set.[31,32] Model stacks are built by superimposing HATNA-SH molecules, separated by 3.4 Å, without any further structure optimization. The theoretical UPS spectra of the isolated molecule and of stacks containing from two to six molecules have been simulated with the help of the intermediate neglect of differential overlap (INDO) semiempirical Hartree−Fock method developed by Zerner and coworkers.[33] The general procedure used to calculate the UPS spectra has been described in detail elsewhere.[34] Briefly, we simulate the spectra within Koopmans' approximation (i.e., using eigenvalues as binding energies), without estimating cross sections, and by matching the HOMO of the single molecule to the experimental spectrum obtained for the disordered phase in order to account for solid-state polarization effects. For the single HATNA-SH molecule, the energy scale has been contracted by a factor of 1.3 to compensate for the neglect of intramolecular electronic relaxation and correlation effects, as used and justified in previous studies.[34] The broadening of the UPS features is introduced with the help of Gaussian functions (with a full-width at half-maximum set at 0.3 eV if not otherwise stated) centered on each eigenvalue.

The angle dependence of the photoelectron emission of the HATNA-SH molecule is simulated within the independent atomic center (IAC) approximation developed by Grobman.[29] This type of analysis has been shown to be reliable in determining the orientation of large conjugated molecules such as phthalocyanines[35] and bis(1,2,5-thiadiazolo)-*p*-quinobis(1,3-dithiole) (BTQBT) deposited on graphite,[36] or In-[perylene-3,4,9,10-tetracarboxylic dianhydride] on MoS_2.[37] In this model, photoelectrons are considered to be coherently emitted from all the atoms involved in a given molecular orbital of the HATNA-SH core. Note that our simulation does not take into account here the alkane side chains. Since the analysis spot of the experiments probes a surface area of about 1 mm × 1 mm on the samples, the photoemission signal is expected to originate from a multitude of orientations of the molecules along the azimuthal angle. Therefore, the calculated ARUPS spectra have been integrated over the molecular azimuthal angle ϕ_m in the range 0°−360° in 3° steps. The molecular azimuthal angle ϕ_m defines the rotation of the molecular axis (*x*,*y*,*z*) with respect to the fixed axis *a* on the surface of the substrate. As for the experiments, we set the photon polar angle at $\theta_p = 80°$ and $\phi_p = \phi_e$. The total amplitude A_{tot} of the photoemission from the *n*th molecular orbital is given by

$$A_{tot}(\mathbf{R}) = \frac{e^{ikR}}{R} \sum_a C_{na}\, e^{-ikR_a} N_a(\hat{\mathbf{k}}) \qquad (1)$$

The first term is the damping factor of spherical waves at the detector position $\mathbf{R}$ ($=R\hat{\mathbf{R}}$). The sum over the contributions from each individual atom *a* yields A_{tot}. C_{an} is the linear combination of atomic orbitals (LCAO) coefficient of the *n*th molecular orbital on atom a, as provided by the INDO calculations performed on a single HATNA-SH molecule. The term e^{-ikR_a} is the phase factor taking into account the difference in the path length to the detector from each atomic position R_a, with $\mathbf{k}$ ($=k\hat{\mathbf{R}}$) being the wavevector of the photoelectron. The factor $N_a(\hat{\mathbf{k}}) = \sum_{l,m} M_{l,a}^m y_l^m$ is the so-called atomic factor, with $M_{l,a}^m y_l^m \propto \langle \phi_{E_{kin},k} | \hat{\epsilon}\cdot\mathbf{r} | \phi_{nlm} \rangle$. The right-hand term is the transition dipole moment for the optical excitation from the initial state ϕ_{nlm} to the final continuum state $\phi_{E_{kin},k}$ of kinetic energy E_{kin} and wave vector $\mathbf{k}$. $\hat{\epsilon}$ [$=(\epsilon_x,\epsilon_y,\epsilon_z)$] represents the direction of the photon polarization. The full expression of the atomic factor has been described elsewhere and depends on the angles specifying the photoemission direction and the polarization direction of the incident photons.[29,36]

4. Results and Discussion

4.1. Molecular Order in "As-Prepared" Films. Figure 2 displays the experimental ARUPS data for "as-prepared" films (just after the solvent has evaporated) deposited on highly

(31) Lee, C.; Yang, W.; Parr, R. G. *Phys. Rev. B* **1988**, *37*, 785−789.
(32) Becke, A. D. *J. Chem. Phys.* **1993**, *98*, 1372−1377.
(33) Zerner, M. C.; Loew, G. H.; Kichner, R. F.; Mueller-Westerhoff, U. T. *J. Am. Chem. Soc.* **1980**, *102*, 589−599.
(34) Cornil, J.; Vanderdonckt, S.; Lazzaroni, R.; Santos, D. A. d.; Thys, G.; Geise, H. J.; Yu, L. M.; Szablewski, M.; Bloor, D.; Lögdlund, M.; Salaneck, W. R.; Gruhn, N. E.; Lichtenberger, D. L.; Lee, P. A.; Armstrong, N. R.; Brédas, J. L. *Chem. Mater.* **1999**, *11*, 2436−2443.
(35) Kawaguchi, T.; Tada, H.; Koma, A. *J. Appl. Phys.* **1994**, *75*, 1484−1492.
(36) Hasegawa, S.; Tanaka, S.; Yamashita, Y.; Inokuchi, H.; Fujimoto, H.; Kamiya, K.; Seki, K.; Uneo, N. *Phys. Rev. B* **1993**, *48*, 2596−2600.
(37) Azuma, Y.; Akatsuka, S.; Okudaira, K. K.; Harada, Y.; Ueno, N. *J. Appl. Phys.* **2000**, *87*, 766−769.

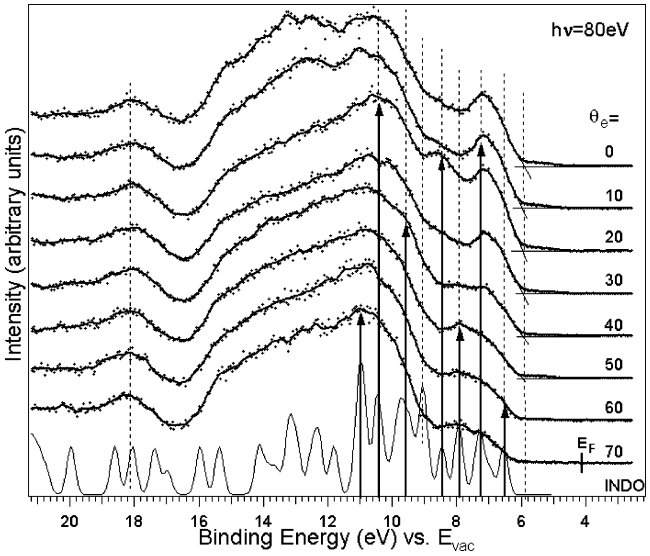

Figure 2. INDO-simulated UPS spectrum (bottom curve) of a single HATNA-SH core and ARUPS valence level spectra of a HATNA-SC_6 film deposited on HOPG just after evaporation of the solvent. The photon beam ($h\nu$ = 80 eV) hits the surface at grazing incidence (θ_p = 80°); the distribution of the photoelectrons from the valence levels is characterized by tuning the polar angle θ_e. The binding energies are relative to the vacuum level (E_{vac}). The theoretical spectrum is obtained by matching the position of the HOMO level to the first ionization potential in the experimental spectrum and by contracting the energy scale by a factor 1.3 to account for correlation and relaxation effects. A Gaussian function is centered on the calculated INDO eigenvalues to simulate solid-state broadening.

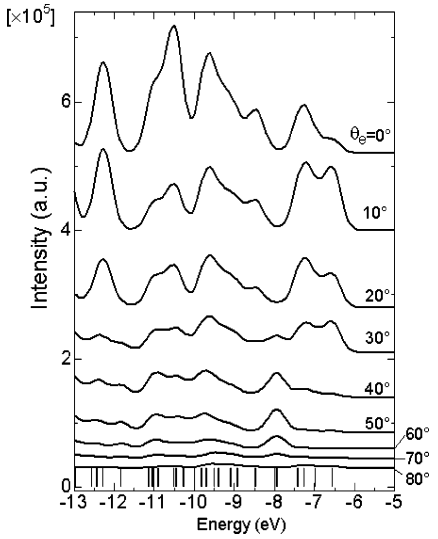

Figure 3. Calculated ARUPS spectra of a single HATNA-SH molecule in the independent atomic center (IAC) approximation. The molecular tilt angle β is set to 12°. The photoemission signal is integrated over the molecular azimuthal angle ϕ_m. The theoretical spectrum is obtained by matching the position of the HOMO level to the first ionization potential in the experimental spectra. A Gaussian function is centered on the calculated INDO eigenvalues to simulate solid-state broadening.

oriented pyrolytic graphite (HOPG), as well as the calculated electronic structure of the core portion of a single HATNA molecule. The onset of the lowest UPS feature occurs at 5.9 eV, while the calculated HOMO is at 6.5 eV after the rigid shift. Although the theoretical value is subject to caution due to the use of Koopmans' theorem and the simple account of polarization effects, we estimate the line width of this feature to be 0.6 ± 0.2 eV from the comparison of the theoretical and experimental spectra. The HOMO is doubly degenerate and delocalized over the conjugated core. The ARUPS shows one feature at 7.2 eV attributed to a sum of contributions from the HOMO−1, doubly degenerate HOMO−2, and HOMO−3 levels, all of which are π-levels delocalized over the conjugated core. This signal increases for lower emission angles θ_e and reaches its maximum around 10°. In contrast, the peak seen at 8 eV corresponds to σ-type orbitals, the doubly degenerate HOMO−4 and HOMO−5 levels, arising mainly from the nitrogen lone pairs. The UPS features associated to these σ-orbitals display a maximum at 50°. The peak at 8.5 eV in the INDO spectrum originates from the HOMO−6 π-level, which is delocalized on the conjugated core (with a significant contribution on the sulfur atoms); it shows a maximum in photoemission intensity at 20°. The strong feature observed in the UPS spectra between 9 and 11 eV originates from both σ- and π-orbitals delocalized on the conjugated core with significant electronic density on the sulfur atoms. When going to higher binding energies, the orbitals acquire a predominant σ-character; it is worth noting that the intensity in the region between 12 and 13 eV is enhanced at low emission angles (0°−10°). The good agreement between the experimental photoelectron spectra and the peak positions in the theoretical simulation obtained for a single conjugated HATNA core indicates that the shape of the photoelectron spectra in as-prepared films is dominated by contributions from weakly interacting molecules.

The ARUPS spectra show some spatial anisotropy for the photoelectron emissions originating from the different orbitals, which implies that a slight preferential molecular order is present in the as-prepared thin films. We have interpreted the ARUPS data within the IAC approximation in order to shed light onto this preferential orientation of the molecules in the film. The best semiquantitative agreement with the experiments is found for a single HATNA-SH molecule tilted by $\beta = 12°$ with respect to the HOPG surface.

We present in Figure 3 the calculated spectra associated with a specific electron polar angle, θ_e, as obtained by integrating the photoemission signal over all the possible azimuthal orientations of the molecule tilted by 12° with respect to the surface. Between 6.5 and 7.5 eV, the frontier π-orbitals (HOMO, HOMO−1, HOMO−2, and HOMO−3) reach their maximum intensity at 10°, and their emission is suppressed at 30°. The σ-orbitals at 8 eV (HOMO−4 and HOMO−5 levels) display a maximum around 40°−50°. The π-orbital HOMO−6, located at 8.5 eV, is visible at low polar angles. However, its maximum at 20°, found in the experiments, is not properly reproduced by the calculations. The region between 12 and 13 eV is enhanced at low emission angles (0°−20°). Note that discrepancies between theory and experiment in terms of peak intensities and angles defining the maximum intensity of peaks might arise due to (i) the low degree of molecular order in the film since molecules oriented randomly remove the sharpness of the experimental photoemission angle dependence,[38] and (ii) the theoretical approximation that is to neglect the scattering phenomena in the ARUPS simulation.[39,40]

(38) Morikawa, E.; Saile, V.; Okudaira, K. K.; Azuma, Y.; Meguro, K.; Harada, Y.; Seki, K.; Hasegawa, S.; Ueno, N. *J. Chem. Phys.* **2000**, *112*, 10476−10481.
(39) Hasegawa, S.; Inokuchi, H.; Seki, K.; Ueno, N. *J. Electron Spectrosc. Relat. Phenom.* **1996**, *78*, 391−394.

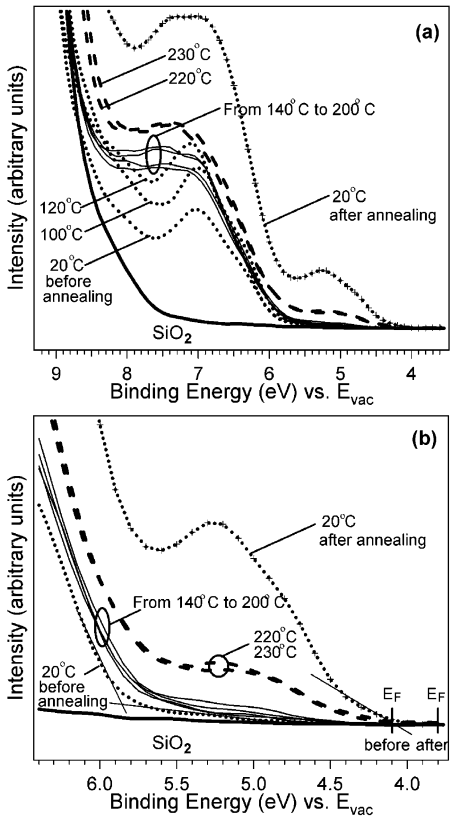

Figure 4. Angle-integrated UPS spectra showing the modification in the upper part of the valence band of a HATNA-SC6 film deposited on SiO_2 upon the annealing−cooling treatment. The binding energies are relative to the vacuum level (E_{vac}). Note that all the spectra collected in this figure are normalized with respect to the intensity of the peak at 11 eV. (b) Enlargement of the low-binding-energy region of (a), where the position of the Fermi level is indicated before and after annealing.

The close similarity between these simulations and the experimental observations indicates that, although a high degree of disorder is present in the as-prepared films, some molecules have a preferential orientation in which the conjugated cores are slightly tilted ($\beta \approx 12°$) with respect to the HOPG surface.

4.2. Change in the Electronic Structure upon Annealing. HATNA-SC_6 is known to undergo a bulk phase transition from a crystalline phase (K) to a liquid crystal columnar mesophase (LC) at 206 °C under atmospheric pressure.[30] Annealing of the partially ordered organic thin film up to the LC transition temperature is thus expected to help the film self-organize in its liquid crystal columnar mesophase. A subsequent cooling to room temperature should provide a crystalline columnar phase where the free enthalpy of the system is minimized. Figure 4 shows the evolution upon heating of the angle-integrated UPS (He I) spectrum of the organic thin film deposited on SiO_2 in the low-binding-energy region. We stress that dewetting and/or formation of pinholes take place in thin organic films spin-coated on HOPG substrates at a temperature slightly above the transition temperature, thus allowing for a possible contribution of the substrate in the spectra; the SiO_2 substrate is chosen here on the basis of the fact that its electronic density of states (DOS) does not appear in the energy region of the π-orbitals of the discotic molecule. The electronic structure of the discotic molecules in the as-prepared sample (dotted line) represents the starting point of the experiment and is similar to that described in Figure 2 on the HOPG substrate. As discussed above, the spectrum shows the electronic signature of weakly coupled discotic molecules, with the HOMO level located at 6.5 eV in the shoulder of the lowest binding energy peak. Raising the temperature from 20 to 120 °C leads to an increase in the intensity of the feature around 7.2 eV (see dotted lines) without changing the global shape of the spectrum. This evolution might be related to a change in the orientation of the alkyl chains close to the surface. Indeed, at room temperature, the alkyl chains of discotic molecules are known to be oriented toward the surface,[41] thus screening the conjugated cores from being seen in UPS. Due to the lower number of neighboring molecules at the surface compared to the bulk, alkyl chains could start melting at the surface at a lower temperature than in the bulk. In this way, they could unprotect the conjugated cores at high temperatures and make them more visible in the UPS spectrum.

Between 140 and 200 °C, the electronic structure (full lines) changes in the energy range between 7.2 and 8.7 eV, as evidenced by the fact that the valley previously observed at 7.7 eV is now filled. Beyond 210 °C, the intensity in the 7.2−8.7 eV region is further enhanced; moreover, a new peak appears in the gap of the disordered film around 5.5 eV (dashed lines). We attribute this new electronic feature to the formation of columns in the LC phase and the simultaneous formation of orbitals delocalized over several molecules rather than localized on a single molecule (vide infra). Cooling the sample to room temperature in its crystal columnar phase increases significantly this low-binding-energy contribution and leads to the appearance of a valley around 8.2 eV (crossed line). We stress that several annealing−cooling cycles performed around the transition-phase temperature shows the reversibility of the process, as confirmed by the systematic appearance of the valley at 8.2 eV characteristic of the K ↔ LC transition. The main feature of the ordered K phase at 20 °C is thus a new photoemission signal lying between 4 and 6 eV, i.e., in the electronic gap of the cast (disordered) film. The onset of this new peak (Figure 4b) yields an ionization potential of 4.1 eV, i.e., 1.8 eV lower than in the disordered phase before annealing. To our knowledge, this is the first time that such a large variation in ionization potential has been reported upon ordering of an organic material. During the cooling step, the increase in intensity of the new UPS feature is attributed to an increase in the number of molecules involved in stacks with a good spatial overlap between the π-orbitals of adjacent conjugated cores. This is expected when going from the LC to the K phase as a result of the attenuation of the geometric fluctuations within the columns.[42] Note that the work function of the organic layer decreases from 4.1 to 3.8 eV after annealing (which is why two different E_F values have been reported in Figure 4b). Hence, the ionization potential of the annealed organic layer becomes very close to its work function. Since all experiments were performed in ultrahigh vacuum, a material with such a low ionization potential does not have an opportunity to react with dioxygen.

The changes in the electronic structure upon heating and cooling cannot be explained by quantum-chemical calculations

(40) Ueno, N.; Kitamura, A.; Okudaira, K. K.; Miyamae, T.; Harada, Y.; Hasegawa, S.; Ishii, H.; Inokuchi, H.; Fujikawa, T.; Miyazaki, T.; Seki, K. *J. Chem. Phys.* **1997**, *107*, 2079−2088.

(41) Hiesgen, R.; Schönherr, H.; Kumar, S.; Ringsdorf, H.; Meissner, D. *Thin Solid Films* **2000**, *358*, 241−249.

(42) Herwig, P.; Kayser, C. W.; Müllen, K.; Spiess, H. W. *Adv. Mater.* **1996**, *8*, 510−513.

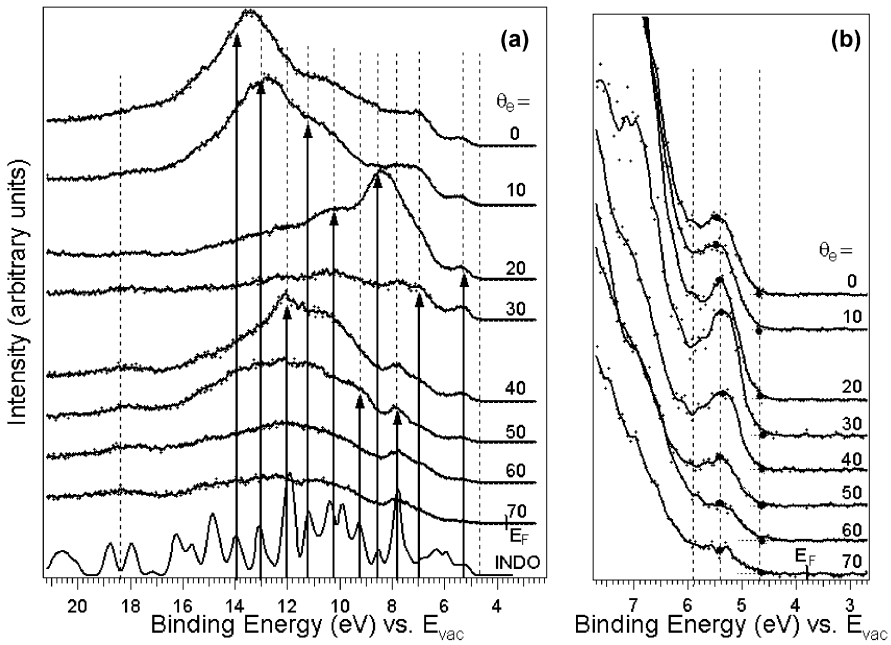

Figure 5. (a) Angle-resolved UPS spectra of the HATNA-SC_6 film deposited on HOPG after the annealing−cooling treatment, i.e., after the transitions from the disordered K phase to the ordered K phase passing by the LC phase. The photon beam ($h\nu = 80$ eV) hits the surface at grazing incidence ($\theta_p = 80°$); the distribution of the photoelectrons from the valence levels is characterized by tuning the polar angle θ_e. The binding energies are relative to the vacuum level (E_{vac}). (b) Enlargement of the low-binding-energy region of (a).

performed on a single conjugated molecular core. However, since the SiO_2 substrate has no DOS in the region of interest, this new feature can safely be attributed to the organic layer. We note that similar modifications in the electronic structure are observed when the HATNA-SC_6 layer is deposited on other substrates, such as HOPG, Au, Cu_2O, and Ag_2O. A new feature in the forbidden electronic energy gap of the molecule could arise from a degradation mechanism involving UV light or secondary electrons, creating, for example, a radical by bond cleavage. A degradation process can be ruled out by the following experimental observations: (i) the changes observed in the electronic properties when heating the sample to 220°C are not sensitive to the time of UV light exposure; (ii) the new feature at 5.5 eV is never detected at room temperature, before any annealing, even after a long UV light exposure; (iii) the electronic modifications can be observed at room temperature after a heating−cooling cycle undergone in UHV without exposure to UV light; and (iv) X-ray photoelectron spectroscopy, which is also a surface-sensitive technique, does not show the appearance of new C(1s), N(1s), or S(2p) signals expected if bond cleavage were to occur.

4.3. Molecular Orientation after Annealing. Figure 5 displays the angular distribution of the photoelectron emission from the organic film deposited on HOPG following annealing. The low-binding-energy feature (at 5.5 eV) observed for the annealed film when deposited on SiO_2 is well reproduced. The ARUPS pattern is sharp for the σ-orbitals lying between 9 and 14 eV, as well as for the π-orbitals (in the 5−9 eV range). The intensity ratio between the σ- and π-orbital contributions changes dramatically with the electron emission angle (e.g., 20° vs 0°), which underlines the high molecular order obtained after annealing. From the orbital analysis of a five-molecule stack, we assign the spectral features between 5 and 8 eV to π-orbitals delocalized over several molecules in the columns. The lowest binding energy peak (at 5.5 eV) has a maximum intensity at about 20°−30°. The feature appearing as a shoulder at 6.9 eV reaches a maximum in intensity at 20°. The peak visible at 7.9 eV between 70° and 40° and reaching a maximum at 50° is attributed to the emission from σ-orbitals localized on the nitrogen lone pairs, as found in the as-prepared film. The interactions between adjacent conjugated cores in the column do not modify their local character. As is the case for the π-region between 5 and 8 eV, the peak at 8.4 eV shows a maximum at 20°. Above 10 eV, the σ-character becomes predominant and the photoemission originates mainly from orbitals localized over a single molecule. Within the angular portion (70°−20°), the maximum intensity of the σ-orbitals at 11 eV is detected at 40°. Below 20°, the emission is suddenly amplified at 10° and then diminishes toward 0°, where the intensity is shifted to higher binding energies.

The pattern of photoemission from σ-orbitals in organic molecules is sharp when using a photon energy of 80 eV.[29] The photoemission distribution from localized σ-orbitals in the highly ordered annealed film can be compared to the emission pattern calculated on a single molecule. The neglect of the alkane chains in our simulations could cause some slight deviations with respect to the experimental ARUPS spectra since the C−C bonds in the side chains likely have a slight preferential orientation. In contrast, the C−H bonds are expected to be randomly oriented, thus contributing a constant weight to the spectrum for various electron polar angles. The ARUPS spectra of a single HATNA-SH molecule have been calculated for several molecular tilt angles with respect to the surface. The theoretical photoemission pattern (Figure 6) displays the best semiquantitative agreement with the experimental ARUPS spectra when the HATNA conjugated core is parallel to the HOPG surface ($\beta = 0°$). Although the π-orbitals have an intermolecular character in the film, the polar angle of maximum photoemission in the π-region (5−8 eV) of the annealed film measured at 20° is similar to that calculated for the π-orbitals

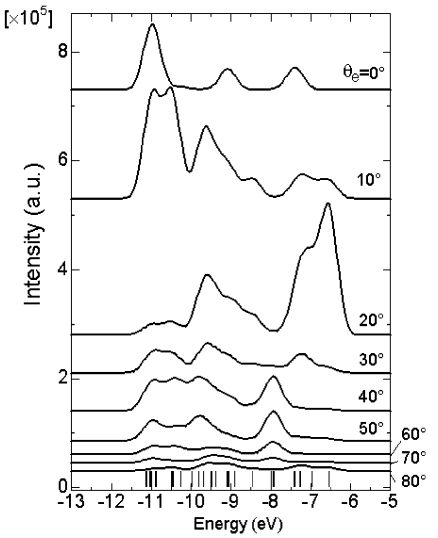

Figure 6. Calculated ARUPS spectra of a single HATNA-SH molecule in the independent atomic center (IAC) approximation. The molecular tilt angle β is set to 0°, i.e., the conjugated core is parallel to the HOPG surface. The photoemission signal is integrated over the molecular azimuthal angle ϕ_m. The theoretical spectrum is obtained by matching the position of the HOMO level to the first ionization potential in the experimental spectra. A Gaussian function is centered on the calculated INDO eigenvalues to simulate solid-state broadening.

(6−8 eV) of a single molecule. The σ-feature originating from the localized nitrogen lone pairs (8 eV) grows from 70° to 40°−50°, and then decreases at lower angles, in agreement with the experimental data. In the range between 70° and 0°, the spectral weight related to the σ-states in the 10−11 eV region reaches a first maximum at 40°, and then is reduced before reaching another maximum at 10°. The very good agreement between the calculated and measured photoemission patterns proves that a high molecular order is achieved after annealing. Moreover, the results indicate that the HATNA-SC_6 molecules likely pack in columns with the conjugated cores parallel to the HOPG surface. Such a preferential orientation in thin films (100−200 Å thick) may be induced by the substrate, as found recently for hexabenzocoronene derivatives deposited on MoS_2.[15]

4.4. Electronic Structure of a Column. The analysis in the section above provides only the tilt angle of the HATNA cores with respect to the HOPG surface. Since the one-dimensional columns could be tilted by any angle τ_c with respect to the HOPG surface, the tilt angle τ_m of the HATNA molecules with respect to the columnar axis is still unknown (Figure 7). Below, we compare the results expected for three different columnar orientations. (i) Structure A: the columns are tilted by $\tau_c = 60°$ (versus the surface normal) on the HOPG surface, the HATNA molecules being then tilted by $\tau_m = 30°$ with respect to the columnar axis. In that case, we calculate a very small HOMO splitting of 0.15 eV (corresponding to a transfer integral of 0.075 eV) in a dimer made of two HATNA molecules with a separation of 3.4 Å between their planes. Structure A modifies the least the electronic structure of individual molecules due to the poor overlap between the electronic wave functions of adjacent units; it is therefore not the most likely. (ii) Structure B: the columns are tilted by $\tau_c = 30°$, the HATNA cores being tilted by $\tau_m = 60°$; here, the electronic coupling between adjacent cores becomes significant and characterized by a HOMO splitting of 0.62 eV. (iii) Structure C: the columns stand

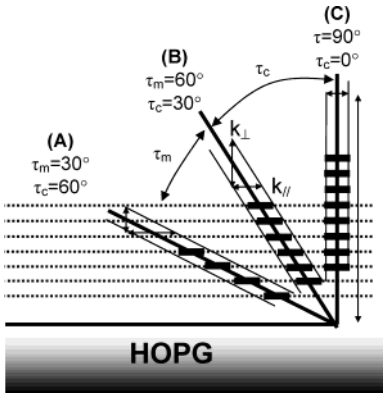

Figure 7. Sketch of the various orientations of the columns with respect to the HOPG surface for a molecular tilt angle $\beta = 0°$ of the HATNA cores. The orientation of the one-dimensional columns is characterized by the tilt angle τ_c relative to the HOPG surface, while the tilt angle τ_m, defined with respect to the columnar axis, specifies the orientation of the HATNA molecules within the columns.

perpendicular to the substrate ($\tau_c = 0°$), the conjugated cores being packed in a cofacial manner ($\tau_m = 90°$); this structure yields the most efficient orbital overlap and leads to a HOMO splitting $2t = 0.99$ eV.

On the basis of these three examples, it is clearly seen that the electronic coupling decreases when the columnar tilt angle τ_c is reduced. This leads to the conclusion that the columns' axes are (nearly) perpendicular to the HOPG surface in order to promote significant electronic coupling between adjacent conjugated cores that generates π-orbitals delocalized over several molecules responsible for the appearance of the low-binding-energy feature in the experimental spectra (Figure 4). This columnar axis orientation is experimentally confirmed by the absence of any energy dispersion of the low-binding-energy feature when the polar emission angle is tuned (see section 4.5). Since the calculated HOMO splitting is quite similar for a column with a slight τ_c tilt, we have considered for the subsequent analysis an ideal stack standing perpendicular to the HOPG substrate (in addition, we have not considered any rotation between adjacent disks[18]). This model maximizes the electronic coupling between adjacent disks and allows for a simple analysis of the electronic structure of the stacks without removing the underlying physics in the actual HATNA-SC_6 columns formed on the HOPG substrate. Note that a rotational angle of 25° between two adjacent HATNA-SC_6 cores provides the energetically most stable columnar organization;[18] this results from a balance between the repulsion of the negatively charged nitrogen atoms of the two adjacent cores and the van der Waals attraction of the alkyl chains. The INDO calculations performed on HATNA dimers show that the HOMO splitting is still significant for such a rotational angle of 25° ($2t = 0.4$ eV at 25° vs 0.9 eV for the cofacial packing).[18] We will come back to this point below.

The INDO-simulated UPS spectra of one-dimensional stacks containing up to six unsubstituted HATNA-SH molecules are presented in Figure 8. The cofacial distance between two adjacent cores is set at 3.4 Å, a value corresponding to the typical intermolecular distance reported for triphenylene-based discotic columns;[43−45] the neglect of the lateral chains in these

(43) Reitzel, N.; Hassenkam, T.; Balashev, K.; Jensen, T. R.; Howes, P. B.; Kjaer, K.; Fechtenkötter, A.; Tchebotareva, N.; Ito, S.; Müllen, K.; Bjornholm, T. *Chem. Eur. J.* **2001**, *7*, 4894−4901.

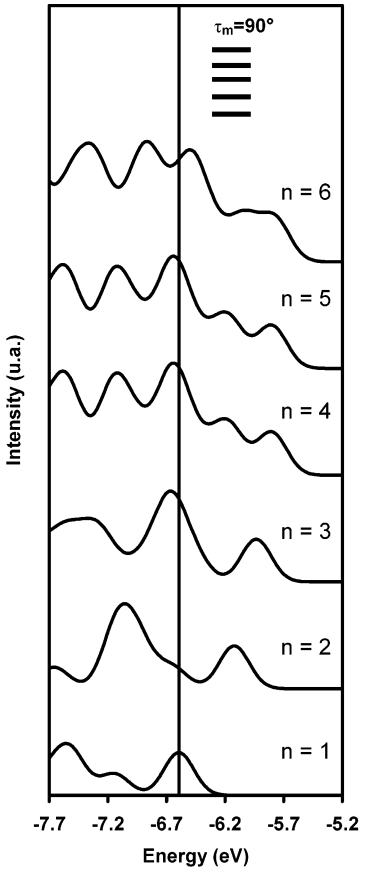

Figure 8. INDO-simulated UPS spectra of one-dimensional stacks (τ_m = 90°) containing from one to six unsubstituted HATNA molecules. The vertical line corresponds to the energy of the HOMO level of the single molecule. Peak broadening is introduced via Gaussian functions (fwhm = 0.2 eV) centered on the orbital energies.

simulations is justified by the absence of σ-molecular orbitals in the low-binding-energy side of the UPS spectra, which is the prime focus of this theoretical section. The results illustrate that the electronic structure of the single conjugated core is strongly modified when the stack progressively builds up and that the energy of the highest occupied orbital saturates after about five molecules. Most importantly, the UPS spectrum simulated for the largest stack rationalizes the appearance of a new feature in the band gap of the single molecule, in full agreement with the experimental spectra obtained upon annealing (see Figure 4). The two highest occupied levels of the single HATNA molecule are degenerate and split in a similar way in stack with cofacial configurations. In such model stacks, the splitting of the two degenerate HOMO levels is estimated to be 0.99 eV for the dimer, corresponding to an interchain transfer integral of 0.49 eV.[25] The HOMO bandwidth is thus extrapolated to be 1.98 eV (i.e., equal to 4*t*) for an infinite stack. The shift of the HOMO level upon going from the isolated molecule to the infinite stack is estimated to be 0.99 eV when changes in the solid-state polarization effects are not considered. However, the increase in electronic coupling upon ordering is expected to promote a higher electronic polarizability of the material,

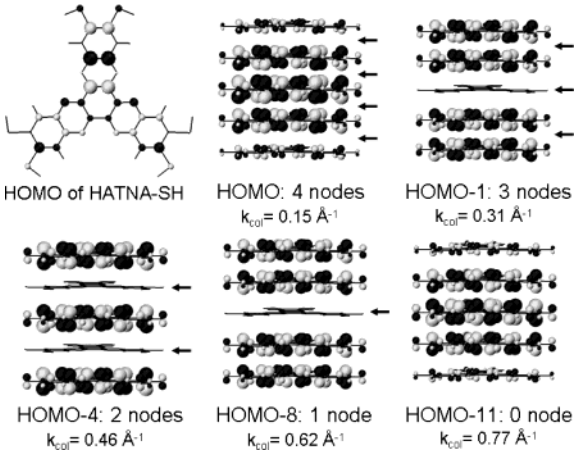

Figure 9. Top view of one of the two degenerate HOMO orbitals in a single conjugated HATNA-SH core (upper-left panel). The other figures represent a side view of the delocalized orbitals in a stack made of five HATNA-SH molecules packed cofacially, as generated by the interaction of the chosen HOMO level of the individual units. The missing levels are associated with the other degenerate HOMO level or with interactions between lower orbitals of the single molecule. The reported quasi-momentum k_{col} corresponds to the value at the intersection between the energy level, represented by a horizontal line, and the tight-binding band dispersion in Figure 10.

hence an increase in the polarization energy that can shift the photoelectron signal of the π-orbitals toward lower binding energies. Such a shift due to a change in polarization energy following a change in molecular packing can exceed 0.3 eV, as reported for perylene crystals.[46] This explains at least partly why the theoretical shift of the HOMO level is underestimated with respect to the experimental reduction in ionization potential by 1.8 eV upon annealing.

To describe the nature of the molecular orbitals in the one-dimensional stacks, we display in Figure 9 the frontier orbitals of a five-unit stack generated by the interaction of the HOMO level of the individual conjugated cores. We focus here only on one of the two degenerate HOMO orbitals since they yield identical splittings in cofacial configurations. The stack orbitals appear to be delocalized Bloch-like functions and display a dispersion behavior typical of electronic band formation: the larger the number of nodes in the interchain overlap, the higher their energy (the lower their binding energy). The HOMO of the stack has a fully antibonding pattern between adjacent conjugated cores (four nodes), while the most stable orbital (HOMO−11 of the stack) shows a fully bonding pattern (without node); these two extreme cases mimic the limits of the first half-Brillouin zone at the scale of an infinite column.

Since the orbitals are delocalized over several molecules in the column, the quasi-momentum of an electron in a given orbital has a component k_{col} along the columnar axis. At the (Hückel) tight-binding level, the energy dispersion for an infinite column is expected to follow a cosine evolution: $E(k_{col}) = \epsilon - 2t\cos(k_{col}d)$, where ϵ is the energy of the level of a single HATNA molecule that creates the band, t the transfer integral, and d the intermolecular separation (3.4 Å). The transfer integral is estimated from the orbital energy splitting, 2t, upon dimer formation.[16,24−26] In the first half-Brillouin zone for an infinite stack (between $k_{col} = 0$ and $k_{col} = \pi/d$), the four π-bands

(44) Allen, M. T.; Diele, S.; Harris, K. D. M.; Hegmann, T.; Kariuki, B. M.; Lose, D.; Peerce, J. A.; Tschierske, C. *J. Mater. Chem.* **2001**, *11*, 302−311.
(45) Gearba, R. I.; Lehmann, M.; Levin, J.; Ivanov, D. A.; Koch, M. H. J.; Baberá, J.; Debije, M. G.; Piris, J.; Geerts, Y. H. *Adv. Mater.* **2003**, *15*, 1614−1618.
(46) Friedlein, R.; Crispin, X.; Pickholz, M.; Keil, M.; Stafstroem, S.; Salaneck, W. R. *Chem. Phys. Lett.* **2002**, *354*, 389−394.

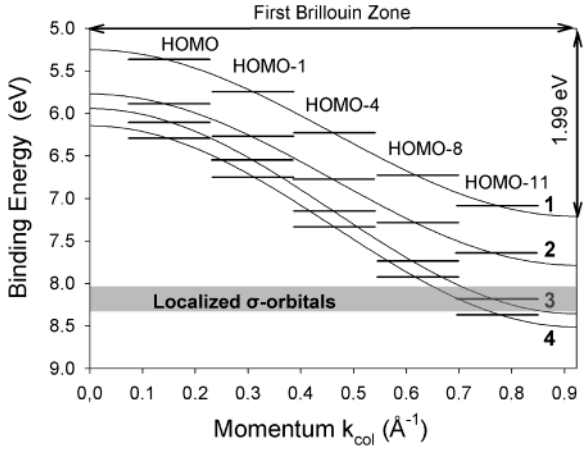

Figure 10. Illustration of the band structure in the upper part of the valence region for an infinite stack as expected from a tight-binding theory. The energy levels (dashes) for a stack of five HATNA-SH molecules packed cofacially and separated by a distance of 3.4 Å are inserted in the band structure. The range of the quasi-momentum associated with each orbital is represented by the lines and obtained as half the fwhm of the function $k^2_{col}s(k)^2$, where s is the structural factor of the system.[47] The first half-Brillouin zone is defined in the momentum range between 0 and $\pi/d = 0.92$ Å^{-1}. The higher energy band is two-fold degenerate and stems from the interaction of the HOMO level of the individual HATNA-SH cores. The second (two-fold degenerate), third, and fourth bands are generated respectively from the HOMO−1, HOMO−2, and HOMO−3 levels of the HATNA-SH molecule. The binding energy scale is obtained with a rigid shift of the calculated orbital energies such that the localized σ-band is at 8 eV, as observed in the ARUPS experiments.

originating from the interaction of the HOMO, HOMO−1, HOMO−2, and HOMO−3 levels of the isolated cores have bandwidths 4t about 1.99, 2.02, 2.42, and 2.36 eV, respectively. These four stack bands are sketched in Figure 10. It is seen that the more stable the band, the larger the bandwidth (or the corresponding transfer integral) since there is a progressive reduction in the number of nodes when going from the HOMO to the HOMO−3 level of the isolated conjugated core.[16] An overlap of the various quasi-bands occurs along the energy scale because the bandwidths are significantly larger than the energy separation between the frontier molecular levels of an isolated HATNA core.

When considering a finite number of repeat units, the calculated orbitals cannot be described by a single wavevector (since k is no longer a good quantum number due to the lack of translational symmetry[47] and each orbital actually translates into a finite width in momentum space). One thus refers here to a quasi-dispersion,[48] with quasi-momenta having the same physical meaning as momenta in infinite systems.[49] The calculated orbital energies for the stack are inserted on the cosine curves (dashes in Figure 10), a procedure that allows estimating the quasi-momentum of the orbitals in the finite-size stack. As expected from Bloch's theorem, valid for an infinite stack, the fully antibonding HOMO level of the stack corresponds to the periodic repetition of the HOMO of the single molecule and is characterized by a value of k_{col} close to 0 Å^{-1}. On the contrary, the fully bonding HOMO−11 of the stack can be produced by repeating the HOMO of a molecule with an inversion of sign on each unit along the stack; the quasi-momentum of HOMO−11 is thus close to the edge of the Brillouin zone at $k_{col} = \pi/d = 0.92$ Å^{-1} for an infinite column.

4.5. Energy Dispersion of the π-Bands. The calculations described in the section above have shown that the shape of the UPS spectrum does not change significantly as soon as a stack made of more than five to six molecular layers is considered. This indicates that a quasi-dispersion should be measured even if the columns are short. ARUPS measurements have demonstrated the formation of π-electronic bands between graphitic planes,[50,51] in organic crystals,[52,53] and in monolayers chemisorbed on metal surfaces (CO on Co,[54] or thione 2-mercaptobenzoxazole, C_7H_5NOS, on Cu[55]). Indications of the delocalized character of states along molecular columns have been pointed out previously.[15,43]

To describe the energy dispersion of the π-bands, we have adopted a three-step model for the photoemission process[56,57] consisting of the consideration of an optical dipole excitation in the bulk, followed by transport to the surface, and emission. We assume that (i) the momentum of the electrons is conserved during the optical transition, and (ii) the final continuum state is a parabolic free-electron-like band in a constant inner potential V_0.[51] V_0 represents the potential step to be crossed by the photoexcited electron to leave the surface. The component $k_\perp$ of the momentum of the photoexcited electron in the solid is[51]

$$k_\perp = \sqrt{2m/\hbar^2}\,(E_{kin}\cos^2\theta_e + V_0)^{1/2} \qquad (2a)$$

$$E_b = h\nu - E_{kin} \qquad (2b)$$

where m is the electron mass and E_b is the binding energy of the electron in the solid. The value chosen for the inner potential V_0 is 14.5 eV; this has been deduced from similar experiments characterizing the inter-plane π-band energy dispersion in HOPG[50] and from low-energy electron diffraction measurements.[58] We believe that it is reasonable to use the same value for the HATNA-SC_6 layer in view of the similar π-electron densities, intermolecular distances (3.40 Å vs 3.35 Å for HOPG),[43−45] and work functions ($W_{HOPG} = 4.1$ eV, $W_{HATNA} = 4.1$ eV).

We focus here on the properties of the low-binding-energy feature. On the basis of the theoretical calculations, this region is associated with π-orbitals delocalized along the columns and is expected to show energy dispersion. The π-band dispersion along $k_\perp$ in the organic layer may be investigated by changing the electron emission angle θ_e or the kinetic energy E_{kin} of the photoelectrons (via the energy of the incident photons), see eqs 2. The ARUPS spectra collected in Figure 5b have been obtained for different emission angles θ_e, using in all cases an incident beam ($h\nu = 80$ eV) hitting the surface at $\theta_p = 80°$ in order to

(47) Narioka, S.; Ishii, H.; Edamatsu, K.; Kamiya, K.; Hasegawa, S.; Ohta, T.; Ueno, N.; Seki, K. *Phys. Rev. B* **1995**, *52*, 2362−2373.
(48) Zojer, E.; Knupfer, M.; Resel, R.; Meghdadi, F.; Leising, G.; Fink, J. *Phys. Rev. B* **1997**, *56*, 10138−10144.
(49) Zojer, E.; Knupfer, M.; Shuai, Z.; Brédas, J. L.; Fink, J.; Leising, G. *J. Phys.: Condens. Mater* **2000**, *12*, 1753−1768.
(50) Law, A. R.; Johnson, M. T.; Hughes, H. P. *Phys. Rev. B* **1986**, *34*, 4289−4297.
(51) Himpsel, F. J. *Adv. Phys.* **1983**, *32*, 1−51.
(52) Hasegawa, S.; Mori, T.; Imaeda, K.; Tanaka, S.; Yamashita, Y.; Inokuchi, H.; Fujimoto, H.; Seki, K.; Ueno, N. *J. Chem. Phys.* **1994**, *100*, 6969−6973.
(53) Yamane, H.; Kera, S.; Okudaira, K. K.; Yoshimura, D.; Seki, K.; Ueno, N. *Phys. Rev. B* **2003**, *68*, 033102−033106.
(54) Greuter, F.; Heskett, D.; Plummer, E. W.; Freund, H. J. *Phys. Rev. B* **1983**, *27*, 7117−7135.
(55) Mariani, C.; Allegretti, F.; Corradini, V.; Contini, G.; Castro, V. D.; Baldacchini, C.; Betti, M. G. *Phys. Rev. B* **2002**, *66*, 115407−111554.
(56) Spicer, W. E. *J. Appl. Phys.* **1969**, *40*, 1395.
(57) Feibelman, P. J.; Eastman, D. E. *Phys. Rev. B* **1974**, *10*, 4932−4947.
(58) Lander, J. J.; Morrison, J. *J. Appl. Phys.* **1964**, *35*, 3593.

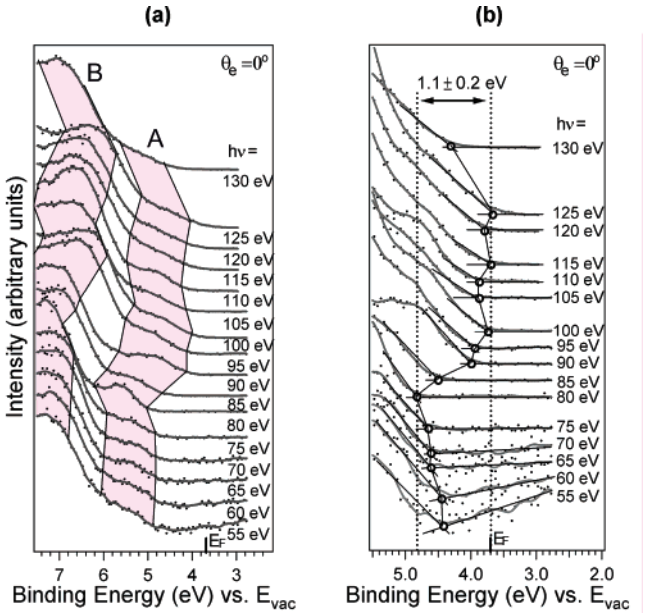

Figure 11. (a) Angle-resolved UPS spectra of the HATNA-SC_6 film in the ordered K phase on HOPG. The incident photon beam hits the surface at grazing incidence ($\theta_p = 80°$), and the photoelectrons emitted normal to the surface are analyzed ($\theta_e = 0°$). The value of the momentum $k_\perp$ is tuned by using different energies for the incident photons. Energy dispersion of two spectral features, A and B, is observed. The binding energies are relative to the vacuum level (E_{vac}). (b) Energy dispersion of the low-binding-energy edge.

promote the maximal photoemission from the π-orbitals in the ordered film. Under those conditions, both $k_{||}$ and $k_\perp$ can change. The value of $k_\perp$ estimated from eq 2a changes marginally (2.0−2.3 $Å^{-1}$) when the detector position θ_e is varied (0°−70°). For columns standing perpendicular to the surface, $k_\perp$ is equal to k_{col}, and the theoretical band structure (Figure 10) predicts that the spectral feature can disperse by up to 0.4 eV for this narrow range of k_{col}. The π-features observed between 5.0 and 6.2 eV show only a weak energy dispersion (0.2 eV), thus confirming that the columns are almost perpendicular to the HOPG surface. Similar observations have been made for other discotic liquid crystal thin films with columns standing on the substrate.[15]

To tune $k_\perp$ and probe the electronic band formed within columns oriented perpendicular to the HOPG substrate, our experimental setup is chosen such that the electrons are collected normal to the surface ($\theta_e = 0°$), while varying the energies of the incident photons. The resulting spectra display two dispersing features, A and B, located around 5.5 and 7.0 eV, respectively (Figure 11a). According to the theoretical models, four dispersing π-bands are expected to lie on the low-binding-energy side of the localized σ-orbital's flat band at 7.9 eV. For all the photon energies, feature A always has a lower intensity compared to feature B. Since the top of the upper band (band 1) has a lower energy than the three lower bands in Figure 10, feature A has a dominant contribution arising from the band generated by the interaction of the degenerate HOMO levels of adjacent HATNA cores. The difference between the onset of feature A (at 4.8 eV) and the energy at the top of band 1 in Figure 10 (5.3 eV) has to be associated with the absence of a proper treatment of the polarization effects in the simulations, as mentioned previously. Feature B would then be formed by the dispersion of the three lower bands (2, 3, and 4 in Figure 10). Note that both features A and B disperse in a similar way,

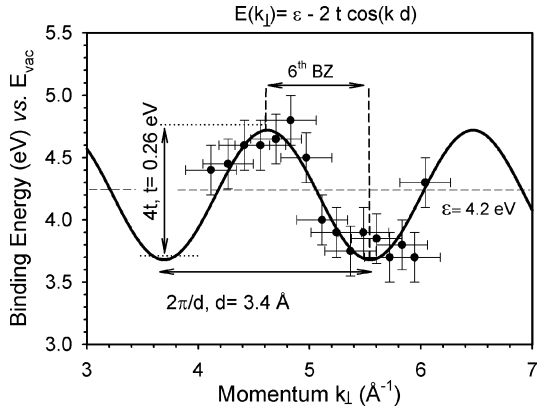

Figure 12. Experimental values of the energy of the band edge as a function of the photon energy are used to plot a band diagram for the upper band using eq 2a. A tight-binding cosine function $E(k_\perp) = \epsilon_{edge} - 2t\cos(k_\perp d)$ fits well the data for an intermolecular distance d set to 3.4 Å. The estimated transfer integral t is 0.26 eV. The energy ϵ_{edge} defines the position of the low-binding-energy edge. According to the calculated values of the momentum $k_\perp$, the experiment probes part of the fifth and sixth Brillouin zones.

which is consistent with the parallel dispersion of the four bands predicted from theory. Since the evolution of feature A is not trivial to follow, we concentrate on its low-binding-energy edge in Figure 11b to probe the dispersion of the upper band. The edge of the dispersed band is expected to shift by a constant value (0.8 eV) with respect to the center of feature A. From the four visible peaks observed at 115, 95, 85, and 70 eV, this difference is 0.8 eV, which is only slightly larger than the 0.6 eV peak width determined previously (as the difference between the center of the HOMO peak, 6.5 eV, and the edge, 5.9 eV, for the nonannealed film, see Figure 2). The energy dispersion of the edge yields an estimate of the bandwidth of 1.1 ± 0.2 eV for the upper band. The measured bandwidth is lower than the calculated value (1.99 eV), suggesting that the molecules do not interact as strongly as in the model columns, as expected from possible molecular rotations along the stacks (see discussion in section 4.4), lateral displacements, and/or fluctuations in intermolecular distances. This experimental value has the same order of magnitude as the inter-planar bandwidth in graphite (1−1.4 eV[50,59]) and is much larger than those estimated in molecular crystals (∼0.5 eV for BTQBT[42] and oligoacenes[60]). Given the ∼1.1 eV bandwidth, it would be of great interest to investigate whether a band regime of transport can actually be achieved in thin films of HATNA-SC_6.

The dispersion of the onset of the upper band is plotted in Figure 12 using eq 2a and the energies of the low-binding-energy edge obtained for various photon energies. As expected from the tight-binding model, a cosine function $E(k_\perp) = \epsilon - 2t\cos(k_\perp d)$ fits the experimental data reasonably well if the repeat unit in the column is made of a single HATNA-SC_6 molecule separated from the adjacent disks by 3.4 Å (this validates the intermolecular distance selected in the calculations). All together, the results suggest that the HATNA-SC_6 columns are highly ordered and maintain a periodicity in the columns, leading to a band following a cosine function. Slight rotational disorder and fluctuations in intermolecular distances and lateral displacements

(59) Marchand, D.; Fretigny, C.; Lagues, M.; Batallan, F.; Simon, C.; Rosenman, I.; Pinchaux, R. *Phys. Rev. B* **1984**, *30*, 4788.
(60) Cheng, Y. C.; Silbey, R. J.; Filho, D. A. d. S.; Calbert, J. P.; Cornil, J.; Brédas, J. L. *J. Chem. Phys.* **2003**, *118*, 3764−3774.

can be responsible for the deviation of the experimental points from a cosine evolution. The band diagram also reveals that the ionization potential (i.e., the energy of the band edge) of the ordered film is only slightly lower than the sample work function (i.e., the Fermi energy), thus suggesting that the columns have a reduced electronic band gap.

5. Conclusions

The electronic structure of hexakis(hexylthio)diquinoxalino-[2,3-*a*:2′,3′-*c*]phenazine (HATNA-SC_6) thin films has been characterized using both angle-integrated UPS and angle-resolved photoelectron spectroscopies (ARUPS) complemented by quantum-chemical modeling. The UPS spectra show that films formed by the rapid evaporation of solvent are composed of molecules in a macroscopically disordered phase where the conjugated cores have a slight preferential orientation on HOPG and are weakly electronically coupled. Subsequent annealing in the liquid crystalline phase (LC) and cooling to the crystalline phase lead to self-organization in columns oriented (nearly) perpendicular to the HOPG substrate on a macroscopic scale. The organized organic thin films display new electronic features in the π-region of the UPS spectra and a lowering in ionization potential by 1.8 eV relative to that of the disordered phase. ARUPS measurements interpreted in the independent atomic center approximation (IAC) indicate that the HATNA conjugated cores are parallel to the HOPG surface.

We have considered stacks made of molecules packed cofacially to better understand the nature of the π-electronic levels in the columns. The electronic structure calculations of such model stacks show that the column formation leads to the appearance of new orbitals in the otherwise forbidden energy gap of the isolated conjugated core, in full agreement with the experimental observations. The theoretical results further illustrate the formation of a quasi-band structure based on Bloch-like orbitals delocalized over several molecules in the column. This is also evidenced by ARUPS data showing large energy dispersion (1.1 eV) of the upper π-band of the columns, thus confirming the delocalized character of the π-electrons. The cosine evolution of the measured energy dispersion implies that columns are highly ordered, with one molecular disk as a repeat unit, and the columnar axis (nearly) perpendicular to the HOPG substrate. The work function of the crystalline columnar phase (3.8 eV) is almost equal to its ionization potential (4.1 eV). The electronic delocalization demonstrated in this work clearly has to be taken into account when describing charge injection into discotic liquid crystals in (opto)electronic devices.

Acknowledgment. We thank Prof. Leif Johansson and Prof. Roger Uhrberg from the Department of Physics at Linköping University for useful discussions. The Mons−Linköping collaboration is supported by the European Commission "Research and Training Network LAMINATE" (project no. 00135). The work in Linköping is supported in general by the Swedish Science Research Council (VR), the Swedish Foundation for Strategic Research (SSF), and an EU-Growth project MACMES (project no. 30242). The work at Georgia Tech is partly supported by the National Science Foundation (CHE-0342321), the Office of Naval Research, and an IBM Shared University Research program. The work at Chalmers is supported by the Swedish Science Research Council (VR). The work in Mons is partly supported by the Belgian Federal Government "Service des Affaires Scientifiques, Techniques et Culturelle (SSTC)" in the framework of the "Pôle d'Attraction Interuniversitaire en Chimie Supramoléculaire et Catalyse Supramoléculaire (PAI 5/3)" and the Belgian National Fund for Scientific Research (FNRS-FRFC). This work was financially supported in Brussels by the Communauté Française de Belgique (ARC no. 00/05-257) and by the European Union (DISCEL G5RD-CT-2000-00321). J.C. is FNRS Research Associate. V.L. and G.K. acknowledge a grant from the "Fonds pour la Formation à la Recherche dans l'Industrie et dans l'Agriculture" (FRIA).

JA048669J